Preprint
UCRL-JC-145741

Recent X-ray Laser Experiments on the COMET Facility

J. Dunn, R. F. Smith, J. Nilsen, J. R. Hunter, T.W. Barbee, Jr., V. N. Shlyaptsev, J. Filevich, J.J. Rocca, M. C. Marconi, H. Fiedorowicz, and A. Bartnik

This article was submitted to:
SPIE International Symposium on Optical Science and Technology, Soft X-ray Lasers and Applications IV, San Diego, California, July 29 - August 3, 2001

U.S. Department of Energy

Lawrence Livermore National Laboratory

September 22, 2001

Recent X-ray Laser Experiments on the COMET Facility

J. Dunn *[1], R. F. Smith [1], J. Nilsen [1], J. R. Hunter [1], T. W. Barbee, Jr. [1], V. N. Shlyaptsev [2], J. Filevich [3], J. J. Rocca [3], M. C. Marconi [4], H. Fiedorowicz [5], and A. Bartnik [5]

[1]Lawrence Livermore National Laboratory, Livermore, CA 94551
[2] Dept. of Applied Science, University of California Davis-Livermore, Livermore, CA 94551
[3] Dept. of Electrical and Computer Engineering, Colorado State University, Fort Collins, CO 80523
[4] Dept. of Physics, University of Buenos Aires, Argentina
[5] Institute. of Optoelectronics, Military University of Technology, 00-908, Warsaw, Poland

ABSTRACT

The development of the transient collisional excitation x-ray laser scheme using tabletop laser systems with multiple pulse capability has progressed rapidly in the last three years. The high small-signal gain and strong x-ray output have been demonstrated for laser drive energies of typically less than 10 J. We report recent x-ray laser experiments on the Lawrence Livermore National Laboratory (LLNL) Compact Multipulse Terawatt (COMET) tabletop facility using this technique. In particular, the saturated output from the Ni-like Pd ion $4d - 4p$ x-ray laser at 146.8 Å has been well characterized and has potential towards a useable x-ray source in a number of applications. One important application of a short wavelength x-ray laser beam with picosecond pulse duration is the study of a high density laser-produced plasma. We report the implementation of a Mach-Zehnder type interferometer using diffraction grating optics as beam splitters designed for the Ni-like Pd laser and show results from probing a 600 ps heated plasma. In addition, gas puff targets are investigated as an x-ray laser gain medium and we report results of strong lasing on the $n = 3 - 3$ transitions of Ne-like Ar.

Keywords: x-ray laser, transient gain, gas puff targets, x-ray imaging, soft x-ray interferometry

1. INTRODUCTION

In recent years x-ray lasers have made rapid progress towards higher efficiency, reduced size, low cost and high repetition rate. These features are scientifically attractive and important for future development of applications that take advantage of the unique characteristics of these sources. Substantial progress has been made in the fast capillary discharge x-ray laser which at the moment is the most compact device. This collisionally pumped Ne-like Ar scheme lases at 46.9 nm in the gain saturation regime and has been extended to high repetition rate, high average power operation [1]. An x-ray laser operating at 10 Hz for a Pd-like Xe ion $5d - 5p$ transition at 41.8 nm was achieved with $gL \sim 11$ using 40 fs irradiation of a xenon gas cell [2]. Tunneling ionization is induced by the high electric field of the intense laser and is followed by pumping of the excited levels by collisional excitation. Very recently, gain saturation has been reported on this scheme [3].

In parallel, the transient scheme as described by Afanasiev and Shlyaptsev has been proposed as a more efficient way of generating laser-driven collisional excitation x-ray lasers [4]. Two laser pulses are utilized where a long nanosecond pulse at $10^{11} - 10^{12}$ W cm^{-2} generates the plasma and creates the required closed shell Ne-like or Ni-like ionization conditions. A delay, depending on the initial plasma conditions, is required for plasma cooling and expansion. This is desirable for both optimum pumping and ray propagation along the plasma column. A second much shorter picosecond laser pulse at $10^{14} - 10^{15}$ W cm^{-2} rapidly generates a transient population inversion. The fast timescale of a few picoseconds for the rapid heating is of order of the collisional redistribution of the excited levels and allows efficient pumping without perturbing the ionization. Very high x-ray laser gains, greater than 100 cm^{-1}, are predicted with the possibility of saturation for target lengths less than 1 cm. The advantage of this scheme is that less than 10 J of laser energy from a chirped pulse amplification (CPA) tabletop laser will drive the inversion where previously 0.1 – 5 kJ was required. The initial experimental demonstration of the transient scheme was shown for Ne-like Ti $3p \rightarrow 3s$ transition at

32.6 nm [5] and was extended to the Ni-like ion sequence for the Pd $4d \rightarrow 4p$ line at 14.7 nm [6]. Gain saturation was reported shortly after on the Ne-like transient scheme for Ti at 32.6 nm and Ge at 19.6 nm using the larger Vulcan-CPA laser at the Rutherford Appleton Laboratory, albeit at higher drive energies of 32 J and 60 J, respectively [7]. Saturated output on the 14.7 nm Ni-like Pd and 18.9 nm Mo x-ray lasers with less than 10 J energy pump in a traveling wave excitation (TWE) was reported at this meeting in 1999 [8, 9]. Further results were published later with simulations of the Pd laser beam divergence and deflection angle parameters [10, 11]. Experimental activity for laser-driven transient gain x-ray lasers has intensified in the last 2 – 3 years at many laboratories including USA, France [12], Japan [13], Germany [14] and the United Kingdom [15]. This scheme has achieved rapid maturity and is an excellent source, when driven into saturation, for applications on account of the unique properties of picosecond pulse duration, high brightness, short wavelength, transverse spatial coherence and high degree of monochromaticity.

In this paper we describe recent experimental progress at LLNL to characterize the parameters of laser-gas puff soft-x-ray lasers (Section 3.). Near-field and far-field imaging results are presented for the Ni-like Pd x-ray laser (Section 4.). Finally we investigate possible applications using transient x-ray lasers and report the first data on picosecond, 14.7 nm interferometry of laser-produced plasmas (Section 5).

2. EXPERIMENTAL DESCRIPTION

The experiments were performed on the Compact Multipulse Terawatt (COMET) laser system at LLNL as described previously [10, 16, 17]. This laser, operating at 1054 nm wavelength, utilizes the technique of chirped pulse amplification to produce three high power beams of nominally 500 fs (compressed) and 600 ps (FWHM) pulse duration with a repetition rate of 1 shot every 4 minutes. A fourth 500 fs beam with a few mJ energy is available as a 1054, 527 or 351 nm wavelength probe. For this work, the short pulse was lengthened to 5 – 6 ps with energy of 4.5 – 6.5 J while the long pulse energy was typically 0.5 J to 4 J. The latter energy was carefully chosen to produce the desired plasma conditions for a particular experiment. For the Ni-like Pd ion x-ray lasers, the peak-to-peak delay between the laser pulses was found to be optimal at 700 ps with the short pulse arriving after the long pulse. These two laser pulses were delivered in a line focus of 1.65 cm long using a cylindrical lens and an on-axis paraboloid [8]. The long pulse was defocused to a width of 150 – 175 μm (FWHM) while the short pulse was focused more tightly to 80 – 120 μm (FWHM). TWE geometry was implemented before the focusing optics by using a high-reflectivity, 0° dielectric-coated reflection echelon consisting of seven flat vertical mirror segments. Each segment was offset by 0.12 cm relative to the adjacent mirror in the direction away from the optical axis of the laser drive beam. (See reference [8] for the experimental setup of the reflection echelon). This introduced a delay of 7.7 ps per step, corresponding to c across the line focus length, matched to the propagation of the x-ray laser in the gain region with a preferred direction towards the flat-field spectrometer. A reflection echelon design was reported previously [18]. The effectiveness of this type of optic for enhancing laser output on different schemes has been documented recently [10, 19]. The third beam had a maximum of 2.5 J energy in 600 ps (FWHM) pulse duration and was used to generate a second plasma in a separate vacuum chamber to be probed by the x-ray laser.

The main diagnostic to monitor the x-ray laser was an on-axis 1200 line mm^{-1} variable-spaced flat-field grating instrument with a back-thinned 1024 × 1024 (pixel size 24 × 24 μm^2) charge-coupled device (CCD) readout. A gold-coated cylindrical and flat mirror collection optic on this spectrometer imaged the plasma across the vertical width of the line focus with 1:1 magnification onto a 500 μm wide entrance slit. Flat polished, high-purity Pd slabs were used to generate the 14.7 nm line. These were tilted back by 2 - 5 mrad in the horizontal direction to compensate for refraction of the x-ray laser in the plasma column. A CCD x-ray slit camera with 25 μm spatial resolution monitored the line focus plasma uniformity and overlap of the laser pulses.

3. GAS PUFF X-RAY LASER EXPERIMENTS

Most of the picosecond laser-driven transient gain x-ray laser experiments have investigated solid target geometry. The advantages of using a gas puff target are numerous: the gas density is closer to the lasing conditions compared to a solid, the initial density can be better controlled and the density gradients in the plasma, in principle, should be more uniform [20]. Other benefits include a high repetition rate with no target debris production. Laser-driven x-ray laser amplification on Ne-like Ar and Ni-like Xe was first demonstrated at MPI in Germany 5 years ago [20] and later repeated for Xe at LULI in France [21]. In these experiments, energies of up to 528 J at 1315 nm in 450 ps pulse or 450 J at 1064 nm in 450 ps, respectively, generated a small-signal gain of 1.65 cm^{-1} with a gL product of 4.5. We first carried out gas-puff experiments on COMET in February 2000 studying Xe and Kr but without success. A follow-up experiment lasting 4 days in 2001 achieved strong amplification on the argon $n = 3 – 3$ transitions and is discussed briefly here.

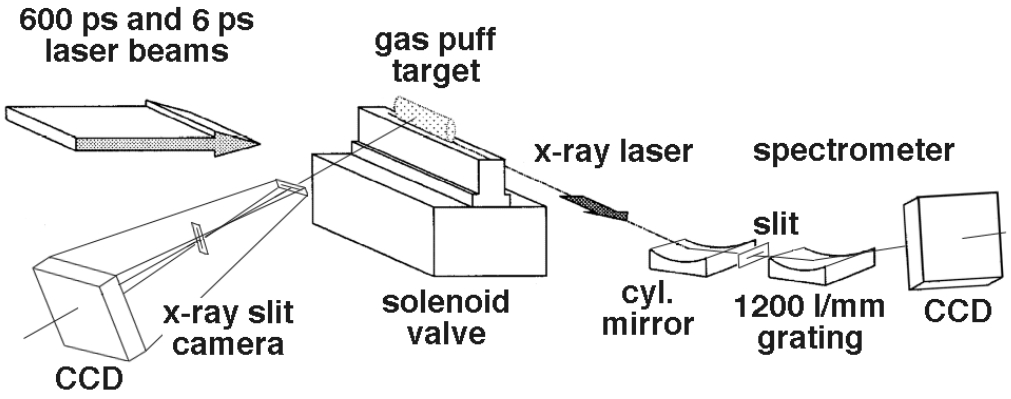

Figure 1: Experimental setup for gas puff x-ray laser experiment.

The experimental setup is shown in Figure 1. The two laser pulses, having a maximum of 4 J in 600 ps and 7 J in 6 ps, were incident on the gas puff in a transverse pumping geometry with TWE irradiation. The gas puff nozzle was 0.9 cm long by 500 μm wide and the laser was focused approximately 150 μm above the nozzle. After an initial parameter scan, the optimum lasing conditions were found for a gas nozzle backing pressure of 10 bar and a valve time delay of 400 μs between the opening of the valve and the laser pulse. The peak-to-peak separation of the laser pulses was varied from 0.5 to 2.1 ns. Figure 2. shows a typical spectrum for a 0.9 cm gas puff target irradiated with 3.84 J, 600 ps pulse followed by 6.26 J, 6 ps pulse. For this shot the laser pulse separation was 1.0 ns. Strong lasing on both $n = 3 - 3$ Ne-like Ar lines at 45.1 nm and 46.9 nm was observed. The lasing intensity was highly sensitive to the experimental conditions, but overall both lines were very reproducible and stable for the optimum conditions.

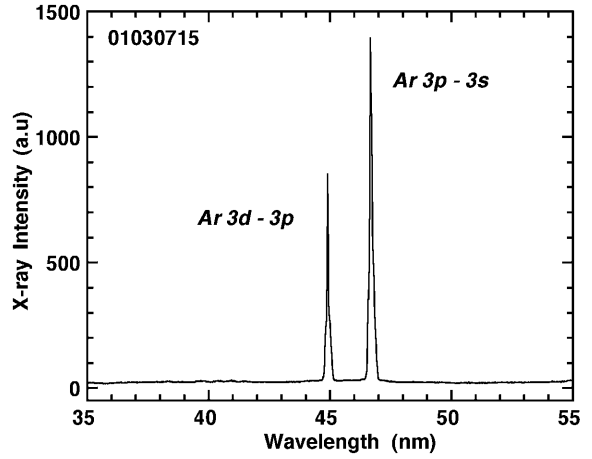

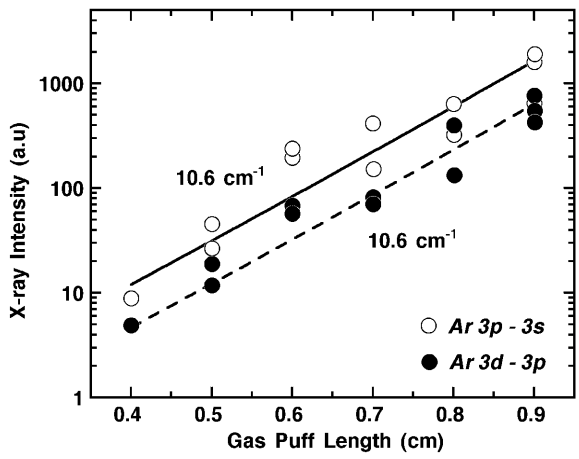

Figure 2: (Left) On axis spectrum from a 0.9 cm argon gas puff. The $3d - 3p$ and the $3p - 3s$ lines at 45.1 nm and 46.9 nm, respectively, are observed.

Figure 3: (Right) Ne-like Ar $3d - 3p$ (closed circles) and $3p - 3s$ (open circles) x-ray laser intensity as a function of plasma length. Fits to the Linford formula are shown for each x-ray laser line with fitted small-signal gain coefficient of 10.6 cm^{-1}.

Figure 3 is a plot of the two laser line intensities versus plasma column length. The gain-length study was performed by blocking the laser drive on part of the gas puff. A small signal gain of 10.6 cm^{-1}, for both the $3d - 3p$ and the $3p - 3s$ x-ray lines at 45.1 nm and 46.9 nm, is estimated by applying the Linford equation to the data points [22]. This yields a gain-length product of 9.6 for each line for a total of ~10 J input pump energy. Further technical details of the experiment

are reported elsewhere [23, 24] and simulations to better understand the laser-coupling, ionization and amplification processes for these gas puff targets are in progress.

4. NI-LIKE PD X-RAY LASER BEAM PROPERTIES

4.1 Near-field beam pattern and far-field beam divergence measurement

The saturated output of the Ni-like Pd $4d \rightarrow 4p$ x-ray laser line at 14.7 nm was characterized in order to optimize the beam properties for the interferometry of dense plasmas discussed in the next section. Previously, we had studied the near-field beam pattern for the saturated output of the Ni-like Mo $4d \rightarrow 4p$ transition at 18.9 nm using multi-layer Mo:Si optics [9, 11]. A similar setup was adopted here as shown in Figure 4. Two x-ray mirror optics, MoC_2:Si multilayers for 14.7 nm wavelength, were used to perform near-field imaging. The 0° spherical x-ray mirror with focal length f =11.75

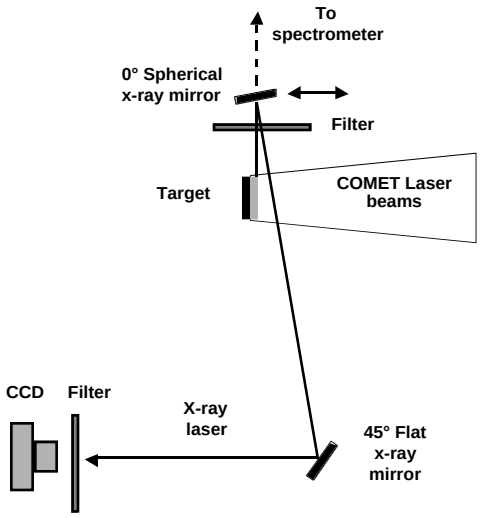

Figure 4: Plan of near-field pattern and spectrometer far field beam divergence measurement. The x-ray laser can be sent to flat-field grating spectrometer to measure the beam divergence in the horizontal plane by translating the spherical mirror. The near-field imaging is achieved by relaying the x-ray laser exit pattern to the CCD camera.

cm was focused to relay image the x-ray laser beam exit pattern via the 45° flat x-ray mirror onto a back-thinned CCD camera. The camera was positioned 248.1 cm from the 0° spherical mirror giving a system magnification of 20.1×. The x-ray laser beam was double-passed through a filter (2000 Å Lexan + 750 Å Al) placed between the target and the 0° mirror. This filter substantially attenuated the x-ray laser signal to prevent saturation of the CCD. An additional light tight filter (2925 Å Zr + 1050 Å polyimide) was placed in front of the CCD camera. The 0° mirror could be translated to allow the x-ray laser beam to be sent to the flat-field spectrometer to measure the far-field beam divergence in the horizontal plane. Thus, the near-field pattern and far-field beam-divergence could be measured under similar laser conditions on alternate shots.

We give an example of the near-field exit pattern and far-field angular divergence below. Further information can be found in ref. [25]. The Pd target length was 1.25 cm irradiated by a 1.65 cm line focus. Laser energy was ~1.25 J in the long pulse and 6.2 – 6.58 J in the 6 ps short pulse. On a technical note, the reflection echelon was set to $0.67c$ TWE and the Pd x-ray laser output was in saturated operation. Figure 5(a) shows a near-field image of the Pd laser beam; the laser beam is incident from the right in the z-direction (horizontal). The aspect ratio of the laser beam is 5× larger in the y-direction (vertical) than the horizontal plane. The dimensions of the laser exit pattern are determined in the horizontal plane by the density gradients in the z-direction away from the target surface and in the vertical plane by the interaction of the short pulse laser with the pre-formed plasma. Figure 5(b) shows a lineout through the near-field pattern along the z-axis. The target surface for this shot is at z=0. It can be seen that the centroid of the emission is approximately 70 μm in front of the target surface with a dimension of 30 μm (FWHM). This latter dimension has been measured to be as small as 22 μm on some shots. The foot of the exit aperture extends uniformly away from the target to more than 150 μm. The overall dimensions are strongly affected by the initial plasma conditions particularly the density gradients and degree of

ionization. Small changes in the long pulse laser intensity e.g. increasing the energy from 1.25 to 1.8 J results in an exit beam pattern that exhibits more structure further in front of the target as a result of density gradients.

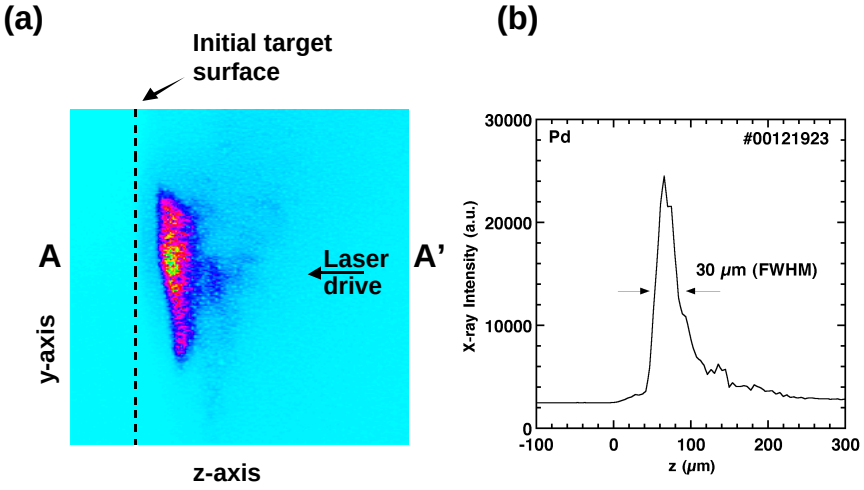

Figure 5: (a) Near-field image of Ni-like Pd 14.7 nm x-ray laser beam as it exits the plasma column. The laser drive is incident from the right. The dashed line shows the approximate position of the initial target surface. (b) Lineout through the center of the image marked AA' in the *z*-direction away from the target.

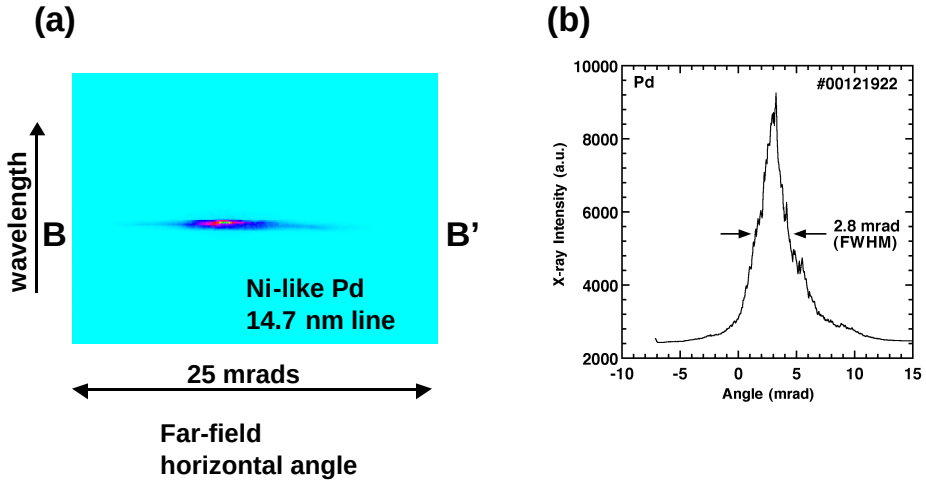

Figure 6: (a) Far-field image from the flat-field spectrometer showing the Ni-like Pd 14.7 nm x-ray laser and angular pointing. (b) Lineout through the center of the image marked BB' showing the beam deflection angle. Divergence is 2.8 mrad (FWHM).

Figure 6(a) shows an image from the flat-field spectrometer taken under similar laser conditions on the previous shot (a few minutes apart) to the near-field image of Fig. 5(a). The far-field horizontal beam divergence can be measured for the laser line. Recently, we reported beam divergence angles of 3 ± 1 mrads (FWHM) and deflection angles of ~3 ± 2 mrad for these plasma conditions for Pd, Ag and Cd $4d \rightarrow 4p$ x-ray lasers [10]. The lineout BB' through the image is plotted in Fig. 6(b) and shows beam divergence of 2.8 mrad (FWHM) with a very uniform shape. Most of the laser energy is in the center part of the beam angular profile with very little structure in the wings. This measurement is close to the 2 mrad (FWHM) reported for saturated output from a 2.3 cm Ni-like Pd x-ray laser driven by a 100 ps pulse [26]. A high degree of x-ray laser collimation is desirable for applications in order to maximize the x-ray laser fluence on the experiment.

Comparisons with the expected geometrical and diffraction limited beam divergence can be made for the x-ray laser source, see discussion in reference [27] for example. The relevant laser parameters for this experiment are wavelength λ = 14.7 nm, an exit aperture $2a \sim 30$ μm, and a column length $l \sim 1.25$ cm. The expected geometrical beam divergence 2θ =

$2a/l \sim 2.4$ mrad is very close to the measured divergence in the horizontal plane. The diffraction-limited divergence for a fully coherent source would be $2\theta = (2/\pi)^{1/2} (\lambda/2a) \sim 0.39$ mrad. This indicates the x-ray laser is operating at 5 – 7× diffraction limit in this study and is therefore partially coherent. The beam exit aperture is expected to consist of a 10 – 100 islands or modes of coherence, with a transverse spatial extent of x_{trans} ~4.5 μm. The x-ray laser horizontal beam divergence in Fig. 6(a) is measured over all vertical rays since the x-ray emission is collected by a cylindrical Au-coated mirror and relay-imaged onto the entrance slit of the spectrometer. An estimate for the x-ray laser longitudinal coherence length l_{coh} is based on the RADEX simulation for a plasma ion temperature of $T_i \sim 80$ eV. A thermal Doppler-broadened line shape with $\lambda/\Delta\lambda \sim 1.495 \times 10^4$ gives l_{coh} ~220 μm. It should be noted that the XRL coherence length is shorter than the x-ray laser pulse duration equivalent longitudinal length of $c\tau_{XRL} \sim 1800$ μm for $\tau_{XRL} \sim 6$ ps

4.2 Far-field beam pattern

The setup shown in Figure 4 was modified to observe the full far-field beam structure of the 14.7 nm Pd line. The 0° spherical multi-layer x-ray mirror was replaced with a flat 0° multi-layer x-ray optic. The CCD was moved closer to the 45° mirror at a distance of 130.4 cm from the end of the target to observe as large as possible angular field of view. The 7-segment TWE reflection echelon was set to 1c. Laser energy on target was ~1.87 J in 600 ps and 6.34 J in 6 ps with the nominal Δt = 700 ps pulse separation. Detailed analysis will be reported in a later publication but we present the results here to supplement the near-field pattern discussion of section 4.1.

Figure 7 shows the x-ray laser 2-dimensional far-field image from a 1.25 cm target: the displayed solid angle is 10 mrad × 15 mrad (H × V). The white square in the bottom right corner is a 1 × 1 mrad^2 reference scale. The far-field profile has larger vertical divergence than horizontal divergence as reported in previous 100 ps driven x-ray laser experiments [28]. The peak intensity is approximately one third from the left hand side. The overall horizontal beam divergence is ~3 mrad (FWHM) and is similar to the measurements in section 4.1. It can be seen that the angular beam profile consists of a few tens of hot spots as a result of modes in the amplifier. The hot spot solid angle is typically less than 1 mrad^2. The intensity, shape and position of these hot spots change from shot-to-shot. Another observation is the presence of faint interference fringes at the right and top of the image; this indicates parts of the beam are coherent and overlapping at the detector plane. The major issue for using this x-ray laser for interferometry is the effect of the mode structure on the transverse spatial coherence across the beam and therefore on the resultant fringe uniformity. Larger more uniform intensity structure in the center of the beam of Fig. 7 is preferable for interferometry than the smaller peripheral structure.

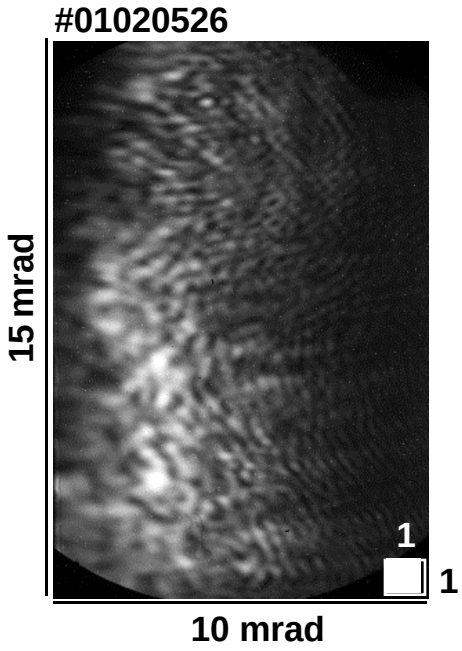

Figure 7: 2-D far-field image of the Ni-like Pd 14.7 nm x-ray laser showing the angular beam profile. The image has a 10 × 15 mrad^2 (H × V) field of view.

5. TABLETOP PICOSECOND X-RAY LASER INTERFEROMETRY

In the last 6 years there has been a number of major advances in the application of x-ray laser interferometry to probe dense laser-produced plasmas [29 - 31]. Da Silva and co-workers with the Nova 15.5 nm Ne-like Y laser first demonstrated the technique with a multi-layer coated Mach-Zehnder interferometer [29]. Large 1-mm-scale plasmas were probed to an electron density as high as 2×10^{21} cm^{-3} to within 25 μm of the initial target surface. Recently, Rocca and co-workers established the 46.9 nm Ne-like Ar capillary discharge x-ray laser as a tabletop interferometric tool using first Lloyd's mirror and secondly Mach-Zehnder diffraction grating instrumentation [30, 31]. Previously in 1978, Attwood *et al.* had successfully demonstrated a 4ω (266 nm wavelength), 15 ps duration probe to determine density profile steepening at high intensities [32]. The use of the 15 ps short pulse duration was essential for probing close to the target surface to freeze plasma motion. A similar advantage of a short pulse x-ray laser will apply with the added bonus of the short wavelength characteristic. The latter allows the x-ray laser to access large plasmas at high density with less deleterious effects of absorption and refraction that strongly limit the applicability of visible or UV probes. The transient

gain x-ray lasers have these properties as well as a few 10s of μJ output energy and high repetition rate. This is sufficient output for applying tabletop picosecond x-ray laser interferometry to laser-produced plasmas.

5.1 Mach-Zehnder type diffraction grating soft-x-ray interferometer description

The Mach-Zehnder type interferometer using diffraction gratings as beam-splitters was designed at Colorado State University [31]. The grazing incidence gratings utilize well-established technology, have high throughput and are robust. This Diffraction Grating Interferometer (DGI) is well matched to the COMET Pd 14.7 nm x-ray laser. The first Au-coated grating *G1*, with 900 l/mm groove spacing, splits the XRL into a 0^{th} order (plasma probe) arm and a 1^{st} order (reference) arm, see Figure 8. The grating blaze angle and geometry has been designed to have equal reflectivity of ~25% in each arm. The two orders are reflected by the long Au-coated mirrors *L1* and *L2* to overlap the arms on the combining grating *G2*. The plasma to be probed is placed in the 0^{th} order beam. The spherical multilayer mirror *S2*, after *G2*, images the plasma and relays the beam via the output Au-coated mirror *L3* to the CCD2 camera. A second ruling of 16 l/mm is machined vertically offset on *G1*, *G2* substrates so that the instrument can be aligned with a 827.1 nm infra-red diode laser, Figure 8. The IR laser was chosen to have similar coherence length to the x-ray laser and allows the adjustment of the various optics to set the two arms equal in length and generate interference fringes. The estimated throughput for each arm, consisting of two grating and one Au-coated mirror reflections, is 0.055. This is 3× higher throughput than the Mach-Zehnder design described by Celliers *et al.* using thin multilayer coated beam-splitters [33].

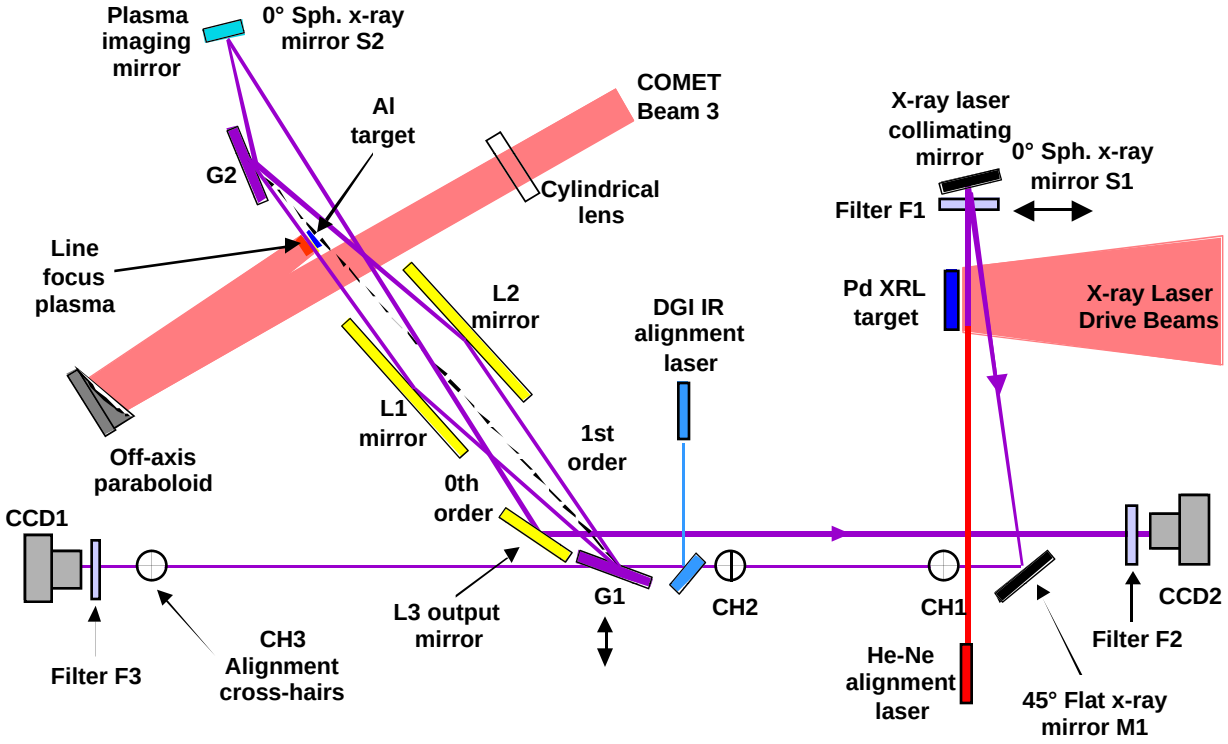

Figure 8: Experimental setup for diffraction grating interferometer on the COMET x-ray laser facility. XRL is collimated by spherical mirror *S1* and sent via flat mirror *M1* along input axis of the DGI onto grating *G1*. XRL pointing is checked on the back-thinned camera CCD1 by translating *G1* out of beam and using cross-hair fiducials *CH1*, *CH2* and *CH3*. *G1* splits beam into 2 orders that are combined at *G2*. COMET Beam 3 with a 600 ps (FWHM) pulse is focused to a line focus on Al target in 0^{th} order arm. Spherical mirror *S2* images plasma and output mirror *L3* routes beam to a back-thinned camera CCD2.

5.2 X-ray laser to diffraction grating interferometer alignment

The complete experimental setup is shown in Figure 8. The XRL output is collimated by the 0° spherical, multilayer x-ray mirror *S1* with focal length f=11.75 cm. This has two advantages: it maximizes the x-ray laser fluence at the plasma to be probed and minimizes the steering of the beam due to variations in the XRL deflection angle as it exits the plasma. The 45° flat mirror *M1* sends the XRL beam along the input optical axis of the interferometer and onto the

first optic grating *G1*. For the initial alignment G1 was translated out to send the beam onto CCD1. The x-ray laser beam pointing is adjusted using the Pd target, *S1* and *M1* to align it to the cross-hair fiducials *CH1*, *CH2*, and *CH3* defining the input axis. Figure 9 shows the image of the x-ray laser beam on CCD1 close to final alignment on the 250 μm cross-hairs. With *G1* installed this collimating arrangement with *S1* gives a defocused but quasi-near-field pattern with ~25× magnification projected at the plasma position. The beam pointing was found to be very stable with shot-to-shot variations of ~50 μrad in angle. This pointing stability is effectively determined by small movements $\Delta z \sim 5$ μm of the XRL beam exit pattern in the z-axis of the Pd target that become magnified by the relay imaging. The Pd z-axis target position, stepper motor encoded in 0.1 μm steps, was used to finely tune the interferogram intensity position at the plasma.

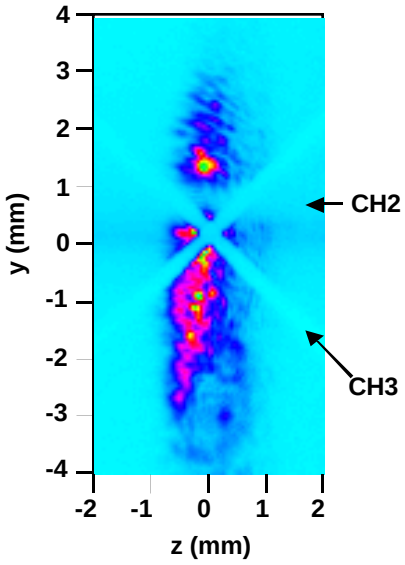

Figure 9: Image from CCD1 showing pointing of the x-ray laser beam along the input optical axis after translating *G1* out of beam. Cross-hairs *CH2* and *CH3* (250 μm wires) are indicated.

The DGI was pre-aligned using the IR laser as discussed in Section 5.1. The COMET Beam 3 was used to generate the plasma. This was imaged by a second spherical multilayer mirror, $f = 25$ cm, and relayed by the Au-coated output mirror *L3* back along the input direction onto CCD2. The magnification of this system was 9.3× giving a pixel limited resolution of 2.6 μm. An additional He-Ne laser was setup to follow the path of the XRL through the interferometer along the 0th arm and to be imaged by spherical mirror *S2* onto the CCD2 camera. Alignment of the main imaging system relative to the Al target position could be verified. Figure 10(a) shows an interferogram at the target plane imaged onto CCD2 without a plasma. The fringes are uniform with some variation in the intensity as a result of mode structure in the beam. Figure 10(b) shows fringe intensity as a function of z position in a lineout through AA'. High quality fringes, set at 18 μm spacing at the target plane, are observed indicating excellent spatial coherence in the laser beam over a large 500×700 μm^2 (H × V) region. High fringe visibility, $V = (I_{max} - I_{min})/(I_{max} + I_{min})$, of 0.72 ± 0.12 is observed.

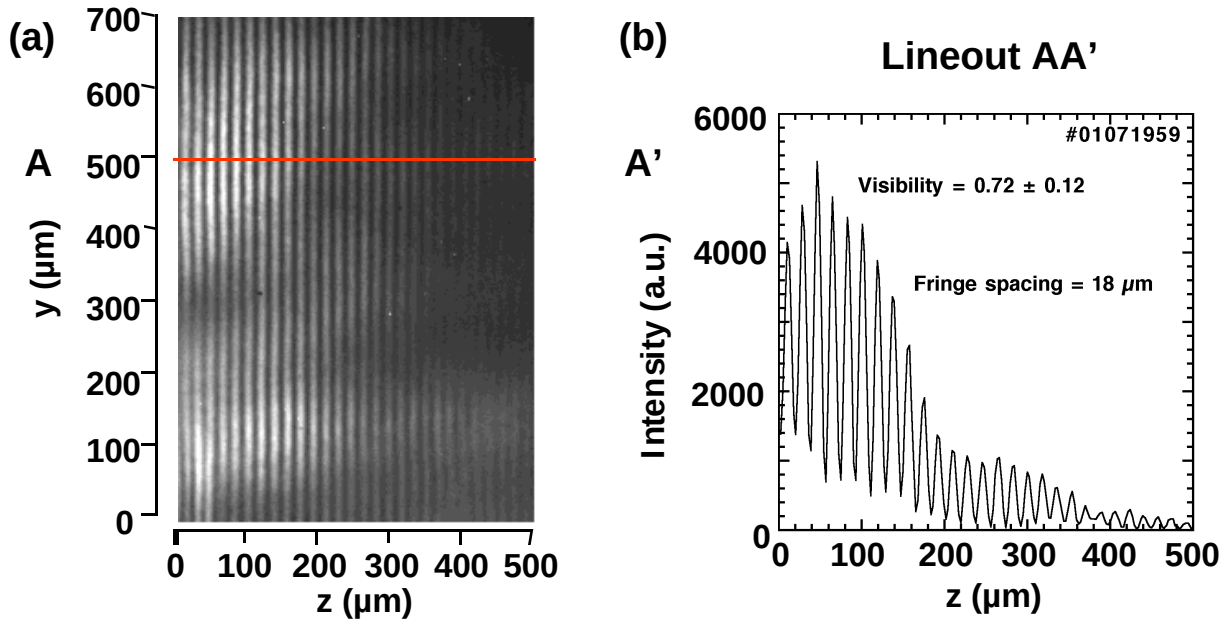

Figure 10: (a) Interferogram of a 500×700 μm^2 region at the target plane. (b) Lineout through AA' at $y = 500$ μm showing high visibility fringe pattern.

5.3 X-ray interferometry results

We report initial results from experiments probing a 0.5 cm long Al slab target heated by the 600 ps (FWHM), 1054 nm laser of COMET Beam 3. A maximum energy of 2.5 J was available to produce a line focus 0.6 cm long using a combination of a cylindrical lens $f = 200$ cm and an off-axis paraboloid $f = 30$ cm. The width of focus was 80 – 90 μm (FWHM) and the laser was at normal incidence to the target. The target rotation angle was carefully adjusted to ensure that the interferometer probe was parallel to the surface. For the data presented below, the laser energy was 0.5 J corresponding to an intensity of 1.7×10^{11} W cm^{-2} on target. A delay line on the plasma-forming beam was adjusted for the x-ray laser to probe the plasma at various times from $\Delta t = 0$ to +2.0 ns, where $\Delta t = 0$ refers to the peak of the heating pulse. The absolute timing of the heating and x-ray laser beams was better than 100 ps while the x-ray laser pulse duration was estimated to be ~6 ps.

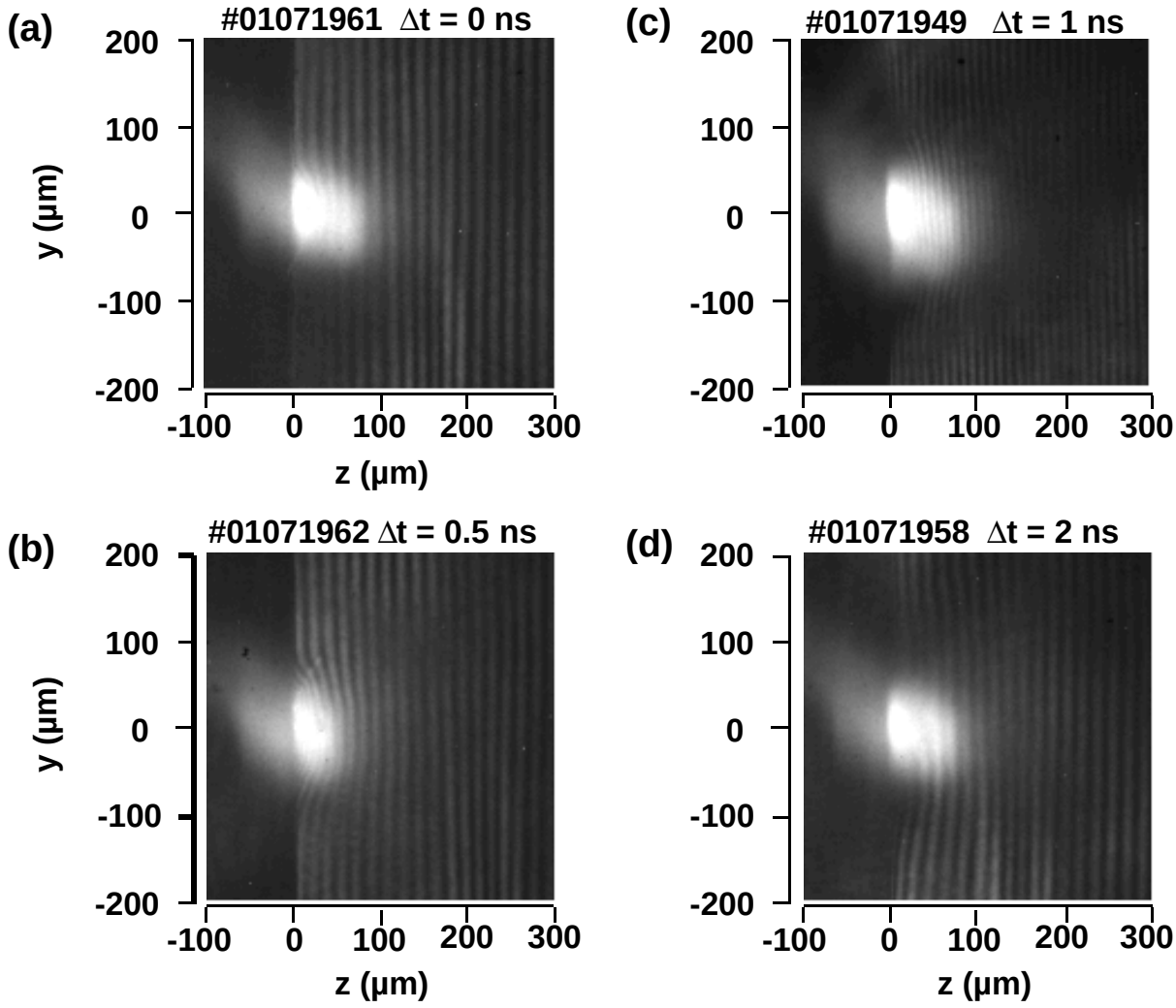

Figure 11: X-ray laser interferograms probing a 0.5 cm Al plasma at various times. Target surface is at $z = 0$. (a) At the peak of the pulse $\Delta t = 0$ ns. (b) $\Delta t = +0.5$ ns. (c) $\Delta t = +1.0$ ns. Note that the fringe spacing is finer on this shot but was adjusted for the other times. (d) $\Delta t = +2.0$ ns .

Figure 11 shows 14.7 nm soft x-ray interferograms of a 400×400 μm^2 imaged region of the Al plasma. The plasma column, being probed end on, extends along the x-axis into the page. Target surface is at z=0 and the bright spot is the time-integrated plasma x-ray emission. Four probe times are shown: Fig. 11(a) for $\Delta t = 0$ at the peak of the plasma forming pulse, and later times Fig. 11(b–d) at $\Delta t = +0.5$, +1.0, +2.0 ns, respectively. The fringe spacing was smaller on an early shot, Fig. 11(c), but was increased for better visibility for the other shots. Fringe shifts due to the presence of the plasma are observed close to the surface at early times. The maximum number of fringe shifts is observed at +0.5 ns

indicating this is the highest density condition, see Fig. 11(b). At later times, +1.0 and +2.0 ns, the heating pulse is off with no further ablation occurring. The plasma continues to expand away from the target in both dimensions well beyond the region of self-emission. In Fig. 11(d) for +2.0 ns, the fringe shift at z = 50 to 70 μm including closer to the surface change direction towards the target indicating a local density peak at this position.

5.4 X-ray interferometry analysis

The critical density, n_{crit} in cm^{-3}, for the probe laser wavelength, λ in μm, is given by the relationship:

$$n_{crit} = 1.1 \times 10^{21} \lambda^{-2} \qquad (1)$$

and corresponds to $n_{crit} = 5.09 \times 10^{24}$ cm^{-3} for the 14.7 nm x-ray laser. For a plasma with electron density, n_e, the index of refraction, n_{ref}, of the plasma is related to n_{crit} by:

$$n_{ref} = \sqrt{1 - n_e / n_{crit}} \qquad (2)$$

This index of refraction due to the plasma in one arm of the interferometer will introduce a fringe shift, N_{fringe}, given by:

$$N_{fringe} = \frac{\delta\phi}{2\pi} = \frac{1}{\lambda}\int_0^L \left(1 - n_{ref}\right) dl \approx \frac{n_e}{2n_{crit}} \frac{L}{\lambda} \qquad (3)$$

where L is the plasma length and the effect of the plasma is integrated along the column length followed by the trajectory

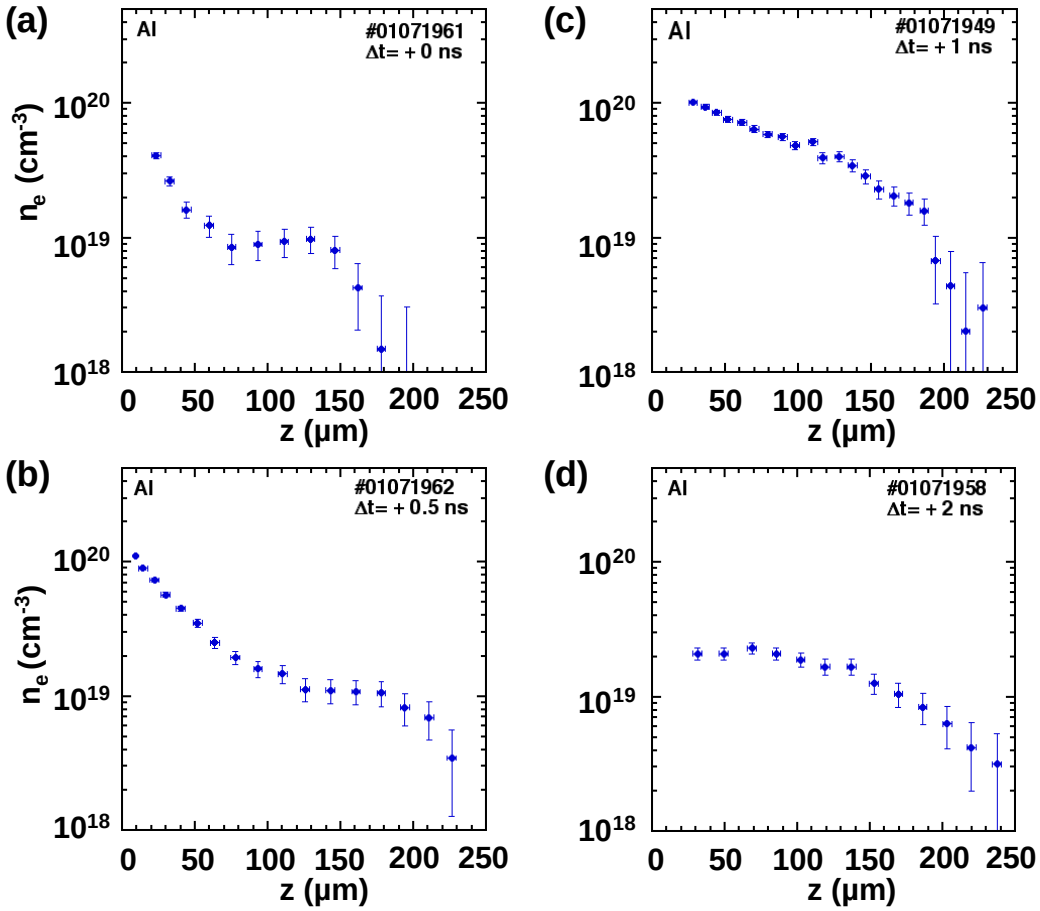

Figure 12: Electron density n_e versus z plots for a lineout through y = 0 for interferograms of Fig. 11. (a) At the peak of the pulse, Δt = 0 ns. (b) Δt = +0.5 ns. (c) Δt = +1.0 ns. (d) Δt = +2.0 ns .

of the probe rays. The fringe shift can be measured over the two-dimensional field shown in Figure 11 and the electron density determined provided the column length is known. Equation (3) can be written as $N_{fringe} = 6.68 \times 10^{20}\ n_e\ L$ (n_e in cm^{-3}, L in cm) and so for 0.508 cm Al targets, one fringe shift corresponds to an electron density of $2.95 \times 10^{19}\ cm^{-3}$.

Figures 12(a–d) are one-dimensional density versus z plots through $y = 0$ for the various probe times shown in Figures 11(a–d). The error bars on the data points result from the uncertainty in the target surface of $\Delta z \sim \pm 5$ μm and a minimum density increment of $\Delta n_e \sim 2.2 \times 10^{18}\ cm^{-3}$ associated with the fringe shift centroid finding method applied here. It can be seen that the plasma expands steadily in time with the steeper density gradients relaxing as time progresses, as expected. The plasma self-emission is brighter than the laser probe and prevents measurements closer than ~15 μm to the target surface. However, 4 fringe shifts corresponding to $n_e \sim 1.2 \times 10^{20}\ cm^{-3}$ at $z = 10$ μm are detected at $\Delta t = +0.5$ ns in Fig. 12(b). The electron density gradient out to $z = 90$ μm indicates a plasma scalelength of 40 μm. Generally, the electron density further out, e.g. $z = 150$ μm, continues to rise for times up to +1 ns after the peak of the heater pulse, Fig.s 12(a–c). Only at later time when the laser pulse is off and no further mass is being ablated and ionized, does the electron density begin to fall, as shown in Fig. 12 (d) at 2 ns. Also, the change in the fringe deflection of the interferogram in Fig. 11(d) is a result of the broad density plateau formed at $n_e \sim 2 \times 10^{19}\ cm^{-3}$ with a gentle roll-off on both sides of $z = 70$ μm.

The effect of refraction on the x-ray laser probe trajectory in the column length is a complicated issue and will be discussed in detail in future work. In light of the density measurements reported here, $n_e \sim 1.2 \times 10^{20}\ cm^{-3}$, and the measured density gradients we expect deflection angles of 1 – 2 mrad leading to deflections of 5 – 10 μm for the probe laser away from the target. We found that the measured deflections were smaller than this when we placed a mesh before the 0.5 cm plasma and backlit it with the 0^{th} order beam. Nevertheless, shorter target lengths would be required to measure higher densities without detrimental effects from refraction. More recent experiments on shorter targets with further reduction of the self-emission have confirmed this and allowed us to probe much closer to the target surface.

6. CONCLUSIONS

We have reported new results from a suite of different experiments performed on the COMET laser over the last 12 months. The goal has been to further develop and understand the transient scheme. More importantly, the transition has been made at our laboratory from source development to applications utilizing these unique, ultra-bright, tabletop sources. Successful picosecond laser-driven amplification on the Ne-like Ar laser lines using the gas puff nozzle developed at the Institute of Optoelectronics has opened another avenue where the initial conditions can be better controlled. Laser heated gas puff plasmas have different properties compared to laser-solid interactions and are being investigated through numerical simulations. The saturated output 14.7 nm Pd x-ray laser has been characterized using near- and far-field imaging techniques. This has given us further insight into the amplification process and the x-ray laser beam properties. Finally, the picosecond x-ray laser interferometry was successfully conducted for the first time using the Mach-Zehnder Diffraction Grating Interferometer designed and constructed at Colorado State University. These initial experiments show that picosecond x-ray laser interferometry is a powerful tool for diagnosing large, hot, dense plasmas and have the potential to benchmark hydrodynamic simulations codes. This is particularly important when the full 2-D plasma density information is extracted from the interferograms. Also, the picosecond x-ray laser interferometer is a unique tool to determine the density profiles of long Ne-like and Ni-like ion plasmas at $n_e \sim 10^{20}\ cm^{-3}$, and will precipitate further understanding of the amplification conditions. In this respect, there is an immediate relevance of this work to the laser-driven x-ray laser community. Further refinements to the experiment and analysis are in progress and will be supplemented with simulations.

ACKNOWLEDGMENTS

The continued support and encouragement of Al Osterheld and Andy Hazi is greatly appreciated. The authors are pleased to acknowledge the technical contributions from Carl Bruns and Al Ellis. These experiments were conducted at the Lawrence Livermore National Laboratory on the Physics and Advanced Technologies Directorate COMET laser facility. This work was performed under the auspices of the U.S. Dept. of Energy by the University of California Lawrence Livermore National Laboratory under Contract No. W-7405-Eng-48, by the U.S. Dept. of Energy grant No. DE-FG03-98DO00208, and in part by grant No. 2 P03B 093 16 of the State Committee for Scientific Research of Poland.

REFERENCES

1. J.J. Rocca, D.P. Clark, J.L.A. Chilla, and V.N. Shlyaptsev, "Energy Extraction and Achievement of the Saturation Limit in a Discharge-Pumped Table-Top Soft X-ray Amplifier", *Phys. Rev. Lett.* **77**(8), pp. 1476-1479 (1996); B.R. Benware, C.H. Macchietto, C.H. Moreno, and J.J. Rocca, "Demonstration of a high average power tabletop x-ray laser", *ibid.* **81**(26), pp. 5804-5807 (1998).
2. B.E. Lemoff, G.Y. Yin, C.L. Gordon III, C.P.J. Barty, and S.E. Harris, "Demonstration of a 10-Hz Femtosecond-Pulse-Driven XUV Laser at 41.8 nm in Xe IX", *Phys. Rev. Lett.* **74**(9), pp. 1574-1577 (1995).
3. S. Sebban *et al.*, "Saturated Amplification of a Collisionally pumped Optical-Field-Ionization Soft X-Ray Laser at 41.8 nm", *Phys. Rev. Lett.* **86**, pp. 3004-3007 (2001).
4. Yu.V. Afanasiev and V.N. Shlyaptsev, "Formation of a population inversion of transitions in Ne-like ions in steady-state and transient plasmas", *Sov. J. Quant. Electron.* **19**, pp. 1606-1612 (1989); V.N. Shlyaptsev, P.V. Nickles, T. Schlegel, M.P. Kalashnikov, and A.L. Osterheld, "Table-top x-ray laser pumped with subnanosecond and picosecond pulses", *SPIE Int. Soc. Opt. Eng. Proc.* **2012**, pp. 111-118 (1993).
5. P.V. Nickles, V.N. Shlyaptsev, M. Kalachnikov, M. Schnürer, I. Will, and W. Sandner, "Short Pulse X-ray Laser at 32.6 nm Based on Transient Gain in Ne-like Titanium", *Phys. Rev. Lett.* **78**(14), pp. 2748-2751 (1997).
6. J. Dunn, A.L. Osterheld, R. Shepherd, W.E. White, V.N. Shlyaptsev, and R.E. Stewart, "Demonstration of X-ray Amplification in Transient Gain Nickel-like Palladium Scheme", *Phys. Rev. Lett.* **80**, pp. 2825-2828 (1998).
7. M.P. Kalachnikov *et al.*, "Saturated Operation of a transient collisional x-ray laser", *Phys. Rev. A* **57**, pp. 4778-4783 (1998); P.J. Warwick *et al*., "Observation of high transient gain in the Ge x-ray laser at 19.6 nm", *J. Opt. Soc. Am. B* **15**(6), pp. 1808-1814 (1998).
8. J. Dunn, Y. Li, A. L. Osterheld, J. Nilsen S. J. Moon, K. B. Fournier, J. R. Hunter, A. Ya. Faenov, T. A. Pikuz, and V. N. Shlyaptsev, "Tabletop transient collisional excitation x-ray lasers", *SPIE Int. Soc. Opt. Eng. Proc.* **3776**, pp. 2– 8 (1999).
9. Y. Li, J. Dunn, J. Nilsen, T. W. Barbee Jr., L. B. Da Silva, A. L. Osterheld, and V.N. Shlyaptsev, "Near Field Imaging of a saturated table top x-ray laser", *SPIE Int. Soc. Opt. Eng. Proc.* **3776**, pp. 45 – 51 (1999).
10. J. Dunn, Y. Li, A. L. Osterheld, J. Nilsen, J. R. Hunter, and V. N. Shlyaptsev, "Gain Saturation Regime for Laser-Driven Tabletop, Transient Ni-like Ion X-Ray Lasers", *Phys. Rev. Lett.* **84**, pp. 4834-4837 (2000).
11. Y. Li, J. Dunn, J. Nilsen, T. W. Barbee Jr., A. L. Osterheld, and V.N. Shlyaptsev, "Saturated tabletop x-ray laser system at 19 nm", *J. Opt. Soc. Am. B.* **17**, pp. 1098 – 1101 (2000).
12. A. Klisnick, *et al*., "Transient pumping of a Ni-like Ag x-ray laser with a subpicosecond pump pulse in a traveling-wave irradiation geometry", *J. Opt. Soc. Am. B* **17**, pp. 1093-1097 (2000).
13. M. Kado *et al.*, "Transient collisional excitation x-ray laser generation with pico-second laser pulses", *Proc. of the 7th Int. Conf. on X-ray Lasers*, in press (2001).
14. K.A. Janulewicz, J. J. Rocca, F. Bortolotto, M.P. Kalachnikov, V. N. Shlyaptsev, W. Sandner, and P. V. Nickles, "Demonstration of a hybrid collisional soft x-ray laser", *Phys. Rev. A.* **63**, pp. 033803 (2001).
15. G. J. Tallents *et al.*, "Short pulse pumped x-ray lasers", *Proc. of the 7th Int. Conf. on X-ray Lasers*, in press (2001).
16. J. Dunn, J. Nilsen, A.L. Osterheld, Y. Li, and V.N. Shlyaptsev, "Demonstration of transient gain x-ray lasers near 20 nm for nickellike yttrium, zirconium, niobium, and molybdenum", *Opt. Lett.* **24**, 101 (1999).
17. J. Dunn, A.L. Osterheld, J. Nilsen, J. R. Hunter, Y. Li, A. Ya. Faenov, T. A. Pikuz, and V. N. Shlyaptsev, "Saturated Output Tabletop X-ray Lasers", *Proc. of the 7th Int. Conf. on X-ray Lasers*, in press (2001).
18. J.R. Crespo López-Urrutia, and E.E. Fill, "Travelling-wave excitation of an X-ray laser medium", *SPIE Int. Soc. Opt. Eng. Proc.* **2012**, 258-264 (1993).
19. R. Tommasini and E. E. Fill, "Effective traveling-wave excitation below the speed of light", *Opt. Lett.* **26**, pp. 689-691 (2001).
20. H. Fiedorowicz, A. Bartnick, Y. Li, P. Lu, and E. Fill, "Demonstration of Soft X-Ray Lasing with Neonlike Argon and Nickel-like Xenon Ions Using a Laser-Irradiated Gas Puff Target", *Phys. Rev. Lett.* **76**, pp.415-418 (1996).
21. D. Ros, H. Fiedorowicz, B. Rus, A. Bartnick, M. Szczurek, G. Jamelot, F. Albert, A. Carillon, P. Jaeglé, A. Klisnick, S. Sebban, P. Zeitoun, "Investigation of XUV amplification with Ni-like xenon ions using laser-produced gas puff plasmas", *Opt. Commun.* **153**, pp.368 (1998).
22. G.J. Linford, E.R. Peressini, W.R. Sooy, and M.L. Spaeth, "Very long lasers", *Appl. Opt.* **13**(2), 379-390 (1974).

23. H. Fiedorowicz, A. Bartnick, J. Dunn, R.F. Smith, J. R. Hunter, J. Nilsen, A.L. Osterheld, and V.N. Shlyaptsev, "Demonstration of a neon-like argon soft x-ray laser using a picosecond-laser-irradiated gas puff target", *Opt. Lett.* in press (2001).
24. H. Fiedorowicz, A. Bartnick, J. Dunn, J. Hunter, J. Nilsen, A.L. Osterheld, R. Rakowski, R.F. Smith, V.N. Shlyaptsev, and M. Szczurek, "Demonstration of a neon-like argon x-ray laser using a short-pulse laser-irradiated gas puff target", *SPIE Int. Soc. Opt. Eng. Proc.* **4505**, in press (2001).
25. J. Nilsen and J. Dunn, "Modeling of short-pulse-driven nickel-like x-ray lasers and recent experiments", *SPIE Int. Soc. Opt. Eng. Proc.* **4505**, in press (2001).
26. R. Tomassini, F. Löenthal, J. E. Balmer, "Saturation in a Ni-like Pd soft-x-ray laser at 14.7 nm", *Phys. Rev. A*. **59**, pp. 1577 (1999).
27. Y. Kato *et al.*, "Development of soft x-ray lasers at the Institute of Laser Engineering: Recent results on Ge soft x-ray laser", *SPIE Int. Soc. Opt. Eng. Proc.* **1551**, pp. 56 – 64 (1991).
28. S. Sebban *et al.*, "Full characterization of a high-gain saturated x-ray laser at 13.9 nm", *Phys. Rev. A*. **61**, pp.043180-1 – 043180-9 (2000).
29. L. B. Da Silva, T. W. Barbee, Jr., R. Cauble, P. Celliers, D. Ciarlo, S. Libby, R. A. London, D. Matthews, S. Mrowka, J. C. Moreno, D. Ress, J. E. Trebes, A. S. Wan, and F. Weber, "Electron Density Measurements of High Density Plasmas Using Soft X-ray Laser Interferometry", *Phys. Rev. Lett.* **74**, pp.3991-3994 (1995).
30. J. J. Rocca, C. H. Moreno, M. C. Marconi, and K. Kanizay, "Soft-x-ray laser interferometry of a plasma with a tabletop laser and a Lloyd's mirror", *Opt. Lett.* **24**, pp. 420 – 422 (1999).
31. J. Filevich, K. Kanizay, M. C. Marconi, J. L. A. Chilla, and J. J. Rocca, "Dense plasma diagnostics with an amplitude-division soft-x-ray laser interferometer based on diffraction gratings", *Opt. Lett.* **25**, pp. 356 – 357 (2000).
32. D. T. Attwood, D. G. Sweeney, J. M. Auerbach, and P. H. Y. Lee, "Interferometric Confirmation of Radiation-Pressure Effects in Laser-Plasma Interactions", *Phys. Rev. Lett.* **40**, pp.184-187 (1978).
33. P. Celliers, T. W. Barbee, Jr., R. Cauble, L. B. Da Silva, C. D. Decker, D. H. Kalantar, M. H. Key, R. A. London, J. C. Moreno, R. Snavely, J. E. Trebes, A. S. Wan, and F. Weber, "Probing High Density Plasmas with Soft X-Ray Lasers", *SPIE Int. Soc. Opt. Eng. Proc.* **3156**, pp. 135 – 145 (1997).

University of California
Lawrence Livermore National Laboratory
Technical Information Department
Livermore, CA 94551